


STRUCTURE-BASED VIRTUAL SCREENING AND MOLECULAR DYNAMIC SIMULATION STUDIES OF THE NATURAL INHIBITORS OF SARS-COV-2 MAIN PROTEASE

<https://palvasha.net/journals/1> 2651-4338

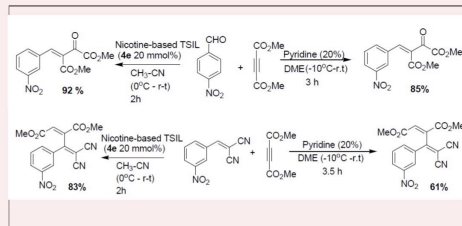
JOURNAL OF ONGOING CHEMICAL RESEARCH

Encouraging Young Chemists

A tidy laboratory means a lazy chemist.
-- Jöns Jacob Berzelius (Swedish chemist, 1779-1848)



Volume 1, Issue 1, 2012, pages 1-61



ongoing Publications

JOURNAL OF ONGOING CHEMICAL RESEARCH

2020

Volume: 5

Issue: 1

Pages: 20-31

Document ID: 2020JOCR42

DOI: 10.5281/zenodo.3767102

Structure-based Virtual Screening and Molecular Dynamic Simulation Studies of the Natural Inhibitors of SARS-CoV-2 Main Protease

Adekunle Babajide Rowaiye*, Olukemi Adejoke Onuh, Rita Maneju Sunday, Zainab Dauda Abdulmalik, Doofan Bur, Nkoli Winifred Emeter, Oluwaseun Adeola Obideyi, Charles Diweni Pelletri, Inikpi Rabi Ujah-Samuel, Chiamaka Rosemary Iwuozor, Priscilla Yahemba Aondona, Victoria Onyayi. Etalong, Nuratu Yussuff, Jude Nnamdi Akpa

[For affiliations and correspondence, see the last page.](#)

Abstract

In the month of December 2019, the outbreak of COVID-19 disease in China marked the beginning of a global health challenge and the urgent need to discover and design appropriate therapeutic agents. The causative agent, SARS-CoV-2 has a high rate of infectivity and its Main protease enzyme plays a major role in the replication mechanism of the virus. This study is aimed at prospecting for natural compounds that have strong binding affinity and the ability to inhibit the SARS-CoV-2 Main Protease. A library of 1,048 natural compounds (with zero violations for Lipinski and Veber rules) obtained from edible African plants were used for this study. These compounds were molecularly docked against the SARS-CoV-2 Main Protease and the results were screened with the docking score obtained from N3 (-7.8 kcal/mol), which is a co-crystallized ligand of the target protein. Further screening for molar refractivity, pharmacokinetic properties and bioactivity was done with *SWISSADME*, *pKCSM*, and *Molinspiration* webservers respectively. The binding site analyses were done using the *PLIP* and *Fpocket* webservers. Molecular dynamic studies and analyses of Apo and Holo structures of target protein were done with the *Galaxy* webserver. The lead compounds, Rhamnetin and Ellagic acid show better therapeutic prediction than the standard. Whilst Rhamnetin binds at the active site, Ellagic acid binds at another cavity with a probable allosteric effect as suggested by the molecular dynamic studies. Further tests are required to evaluate the SARS-CoV-2 Main protease inhibition properties of the lead compounds.

Keywords: Ellagic Acid, Covid-19, Sars-cov-2, Main Protease, Molecular Dynamic Studies, Rhamnetin

INTRODUCTION

The first case of COVID-19 was reported in China in November 2019 and after a month it became an epidemic in Wuhan city, Hubei province, China. By the 30th of January 2020, the World Health Organization declared COVID-19 a Public Health Emergency of International Concern and a pandemic on the 11th of March, 2020. Consequently, many countries of the world have announced emergency health and bio-security guidelines for the containment of the disease (1, 2).

The incubation period for COVID-19 ranges between 2-14 days but 5 days on the average (3). The disease is characterized by symptoms such as fever, dry cough, shortness of breath, sore throat, sputum production,

joint pain, muscle pain, headache, fatigue, loss of smell, loss of taste and pneumonia. Death occurs as a result of multi-organ failure or specifically respiratory failure due to progressing alveolar disease (4, 2) The fatality rate is about 4% mainly causing death in the elderly and the immunocompromised. In spite of the high rate of infectivity, there are no approved vaccines or antiviral drugs for Coronavirus infections (5).

COVID-19 is caused by a novel coronavirus, the Severe Acute Respiratory Syndrome Corona Virus 2 (SARS-COV-2) which is a positive-sense, single-stranded, enveloped RNA virus belonging to the beta-corona sub group of viruses (6). The severe acute respiratory syndrome (SARS) CoV (SARS-CoV) and the Middle East respiratory syndrome (MERS) CoV (MERS-CoV) also belong to this sub-group (7). Generally, Corona viruses infect humans and animals

and they have a size range of 60-80 nm and a genome size of 27-32kb which codes for structural and non-structural proteins (8).

Transmission of COVID-19 is mainly through droplets from infected persons. However, the possibility of blood and faecal-oral transmission has been established. Bats have also been implicated in the zoonotic transmission of SARS-COV-2 (9, 10, 11).

SARS-COV-2 attaches to the host cell through the Spike protein. The S1 domain of the Spike protein binds with the Angiotensin Converting Enzyme 2 (ACE2) which is most abundantly expressed on the type II alveolar cells of the lungs. ACE2 is also expressed in the cells of the gastrointestinal tract (12, 13). The virus invades the nucleus where its nucleic acid alters the host cell genome through gene recombination, deletion or insertion (14). About a third of the modified genomic RNA encodes several structural proteins such as M (membrane), E (envelope), N (nucleocapsid) and S (spike). The other two-thirds of the genome encode for two Replicase polyproteins (ORF1a and ORF1b) which are involved in the viral replication process. Two main proteases namely papain-like protease (PLP) and 3C-like protease (3CL or Nsp5) cleaves the two polypeptides (15, 16).

Virus-encoded proteases have emerged as strategic targets in combating viral diseases. This is because they play a crucial role in the cleaving of high molecular weight poly proteins into functional units necessary for assembly and morphogenesis of new viral particles (17). Therefore, the inhibition of proteases would provide a viable strategy against viral replication. Specifically, cysteine proteases inhibitors possess electrophilic moieties that covalently bind to the cysteine residue of the active site of the target protease. The electrophilic inhibitor fragment of these ligands is incorporated into the substrate binding sites of the protease thereby inhibiting its activity (18). A non-competitive inhibition of the cysteine proteases also occurs when an inhibitor binds to an allosteric site and causes an inactive conformation of the active site resulting in a displacement of the substrate from the enzyme (19).

The Mpro remains a good therapeutic target for drug design because of its strategic function and conserved nature. As a carboxypeptidase and specifically a cysteine protease, Mpro cleaves the C-terminus of replicase polyprotein at 11 sites and transforms it into mature non-structural proteins (20). Though the protein fold is similar to serine proteases, Mpro

cleaves its substrate with the cysteine in its active site and an adjacent histidine residue (21, 22).

In this study, the potential inhibitory activity of small molecules obtained from natural products was investigated. N3 which is a peptidomimetic inhibitor of 6LU7 was used as a reference molecule (23).

RESULTS AND DISCUSSION

Structural analysis, validation and preparation of Main protease (PDB ID: 6LU7): The crystal structure of COVID-19 main protease in complex with an inhibitor N-[(5-Methylisoxazol-3-Yl)Carbonyl]Alanyl-Lvalyl-N1-((1r,2z)-4-(Benzyloxy)-4-Oxo-1-[(3r)-2-Oxopyrrolidin-3-Yl]Methyl}But-2-Enyl)-L-Leucinamide, (N3) (Figure 1 & 2). It has 306 amino acids with the following constituent secondary structures: α helix 23 %; beta sheets 31%; Coil 45%; and Turns 28%. Total Accessible Solvent Area (ASA) is 14043.1(Å)². X ray diffraction study revealed resolution is 2.16 Å and unit cell crystal dimensions are a = 97.931Å, b = 79.477 Å, and c = 51.803Å for α (90°), β (114.55°) and γ (90°) angles respectively. The R-Value is 0.202 and R-free value is 0.235.

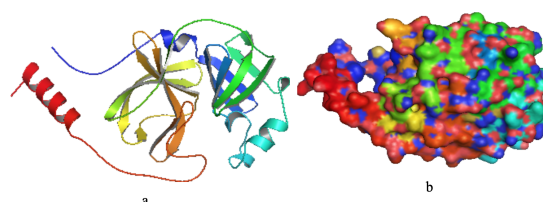


Figure 1. The Crystal structure of MPro of SARS-CoV-2 (PDBID: 6LU7) a: Cartoon representation, b: Surface representations.

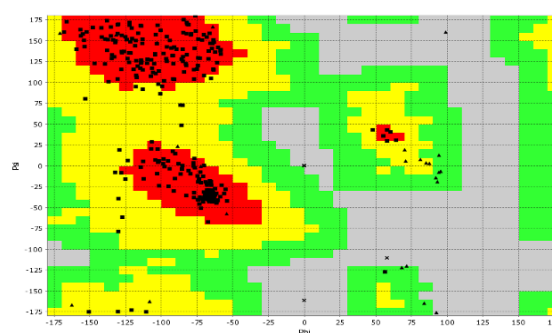


Figure 2. Ramachandran plot for MPro of SARS-CoV-2 (PDBID: 6LU7) Red: Core region; Yellow: Allowed region; Green: Generous region; Grey: Disallowed region; Black squares: Allowed region; Black triangles: Glycine residues; Black X: Disallowed

Ramachandran analysis of the candidate structure shows that 97% of residues are within the favoured region, allowed region is 3% and 0.0% outliers (Figure 2). Rotamer analysis shows that 100% of rotamers are within the favoured region and 0.0 % outliers. The VDW repulsion energy of 6LU7 was minimized by *Chiron* to 42.52 Kcal/mol with a clash ratio of 0.0095.

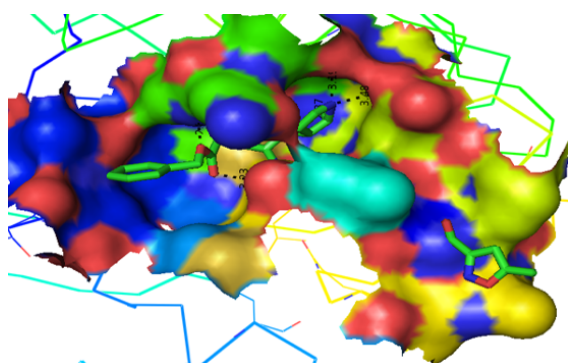


Figure 3. Active site of MPro of SARS-CoV-2 with co-crystallized ligand, N3

Chemoinformatic profile of ligands: The oral bioavailability of drugs depends on several properties as described by Lipinski and Veber rules. A drug should have a molecular weight of less than 500 daltons, a log P (octanol–water partition coefficient) value of less than 5, less than 5 hydrogen bond donors (–OH or –NH groups) and less than 10 hydrogen bond acceptors (O or N atoms in total) (40). In a similar vein, drugs with good oral bioavailability should have 10 or less rotatable bonds and a topological polar surface area of less than 140 Å² (angstroms squared) (41). Another property of drug-likeness is molar refractivity. A range of between 40–130 cm³ is an indication of good oral bioavailability (42).

Table 1. Chemo-informatic properties of standard and lead compounds

	N3 (Standard)	Ellagic Acid	Rhamnetin
Molecular Weight (g/mol)	684.835	302.19	316.26
XLogP3	2.1	1.1	1.9
Hydrogen Bond Donors	5	4	4
Hydrogen bond acceptors	10	8	7
# heavy atoms	6	16	23
# rotatable bonds	18	0	2
TPSA (Åa)	196.88	141.34	120.36
Molar Refractivity	191.34	75.31	82.50
GCPR ligand	-0.28	-0.29	-0.11
Ion channel modulator	-1.33	-0.27	-0.27
Kinase Inhibitor	-1.21	-0.01	0.21
Nuclear Receptor Ligand	-1.17	0.11	0.27
Protease Inhibitor	0.06	-0.18	-0.27
Enzyme Inhibitor	-0.70	0.17	0.20

Ellagic acid and Rhamnetin have no violation of the Lipinski, Veber and Ghose rules indicating potentially good drug permeability (Figure 4, Table 1). However, the standard has a molecular weight that is greater than 500g/mol thereby violating the Lipinski rule for orally administered drugs. The standard also has the number of rotatable bonds higher than 10 and the TPSA greater than 140Å. Molar refractivity of the standard is higher than 130 cm³ making it violate the Ghose rule. In terms of bioavailability, the lead compounds are better than the standard.

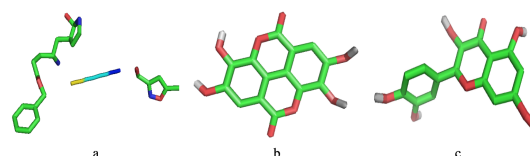


Figure 4. The 3D chemical structures (stick model) of standard and lead compounds a: N3, b: Ellagic acid, c: Rhamnetin

Beyond binding to its target, a potential drug should show bioactivity as predicted by the *Molinspiration* webserver (Table 1). Ellagic acid and Rhamnetin show moderate activity with respect to protease inhibition while N3 shows good activity. On the contrary, the lead compounds show good activity as enzyme inhibitors as compared with N3 which has moderate activity (43).

Pharmacokinetic properties of ligands: Pharmacokinetics plays a critical role in drug discovery and development. Beyond efficacy, a high-quality drug candidate should have good absorption, distribution, metabolism, excretion, and toxicity (ADMET) properties at a therapeutic dose (44). In ADMET studies, critical factors such as bioavailability; rate, mechanism and metabolites of metabolism; rate and mechanism of excretion; and toxic effect of drug candidate are considered.

From Table 2, except for CYP1A2 inhibition, Ellagic acid and Rhamnetin are within the pharmacological range for all the predicted ADMET properties (45). Inhibition of an isoform of cytochrome P450 could cause cellular toxicity of its substrates. Caution must be taken not to administer the lead compounds with CYP1A2 substrates as this would increase the bioavailability of the substrates. Expressed in the intestinal epithelium, the P-glycoprotein 1 is a cell membrane transporter protein that removes drugs and toxic metabolites out of the cells reducing their absorption. Ellagic acid and Rhamnetin are predicted to be substrates of P-glycoprotein which implies that they should be administered with a P-glycoprotein

inhibitor to facilitate their cellular absorption (46).

Table 2. Pharmacokinetic properties of standard and lead compounds

	N3 (Standard)	Ellagic Acid	Rhamnetin
Water solubility (log mol/L)	-4.112	-3.181	-3.212
Caco2 permeability (log Papp in 10 ⁻⁶ cm/s)	0.37	0.335	-0.361
Human Intestinal absorption (% Absorbed)	62.162	86.684	80.214
Skin Permeability (log Kp)	-2.73	-2.735	-2.735
P-glycoprotein substrate (Yes/No)	Yes	Yes	Yes
P-glycoprotein I inhibitor (Yes/No)	Yes	No	No
P-glycoprotein II inhibitor (Yes/No)	Yes	No	No
VDss (human) (log L/kg)	-0.793	0.375	0.419
Fraction unbound (human) (Fu)	0.167	0.083	0.073
BBB permeability (log BB)	-1.671	-1.272	-1.345
CNS permeability (log PS)	-3.812	-3.533	-3.235
CYP2D6 substrate (Yes/No)	No	No	No
CYP3A4 substrate (Yes/No)	Yes	No	No
CYP1A2 inhibitor (Yes/No)	No	Yes	Yes
CYP2C19 inhibitor (Yes/No)	No	No	No
CYP2C9 inhibitor (Yes/No)	No	No	No
CYP2D6 inhibitor (Yes/No)	No	No	No
CYP3A4 inhibitor (Yes/No)	No	No	No
Total Clearance (log ml/min/kg)	0.843	0.537	0.473
Renal OCT2 substrate (Yes/No)	No	No	No
AMES toxicity (Yes/No)	No	No	No
Max. Tolerated dose (human) (log mg/kg/day)	-0.341	0.476	0.56
hERG I inhibitor (Yes/No)	No	No	No
hERG II inhibitor (Yes/No)	Yes	No	No
Oral Rat Acute Toxicity (LD50) (mol/kg)	4.355	2.399	2.453
Oral Rat Chronic Toxicity (log mg/kg_bw/day)	3.391	2.698	2.679
Hepatotoxicity (Yes/No)	Yes	No	No
Skin Sensitization (Yes/No)	No	No	No
T.Pyriformis toxicity (log ug/L)	0.285	0.295	0.331
Minnow toxicity (log mM)	4.91	2.11	1.885

Both lead compounds are better than the standard which is predicted to be an inhibitor of P-glycoprotein I & II and hERG II. A positive hERG prediction implies that potassium ion channel of myocardium can be blocked resulting in disrupted electrical activity of the heart and probably death (47).

Put together the lead compounds are safer and better drug candidates than the standard.

Molecular docking score and binding site analyses:

Molecular docking facilitates non-covalent binding between protein and ligand. It also predicts mode of interaction and binding site of both molecules. A ligand with the lowest binding energy suggests the greatest binding affinity making it a possible drug candidate (48). Results from the molecular docking were screened with the binding affinity of the N3 (standard) with Mpro (-7.8 kcal/mol). Ellagic acid and Rhamnetin have stronger binding affinities with scores of -8.3 kcal/mol and -7.9 kcal/mol respectively (Figure 5).

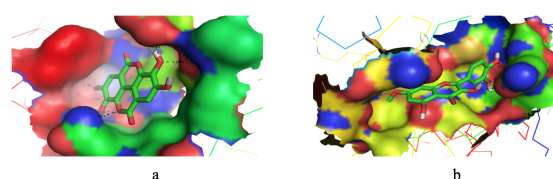


Figure 5. Active site of Mpro of SARS-CoV-2 interacting with lead compounds a: Ellagic acid, b: Rhamnetin

Table 3. Hydrogen bond analysis of Mpro with standard and lead compounds

Compound	Exhaustiveness	Residues	Distance (H-A)	Distance (D-A)	Bond angle
N3 (Standard)	5	GLY143A	2.0	2.87	145.90
		PHE140A	3.62	4.03	108.21
		SER144A	3.65	3.99	104.01
		HIS164A	1.85	2.80	161.75
		GLU166A	2.60	3.48	144.50
Ellagic acid	8	LYS102A	3.31	3.85	115.08
		GLN110A	2.15	3.13	177.90
		THR111A	1.88	2.80	155.30
		THR111A	2.31	2.99	126.48
		ASN151A	3.54	3.90	105.26
		ASP153A	2.49	3.01	115.05
		ASP153A	2.23	3.01	137.37
		SER158A	2.20	3.16	168.22
Rhamnetin	6	PHE140A	3.23	4.10	151.12
		ASN142A	2.82	3.24	107.19
		GLY143A	2.58	3.06	110.13
		SER144A	2.11	2.80	125.70
		CYS145A	2.44	3.12	125.26
		GLU166A	3.06	4.00	159.34

Rhamnetin exhibited (-7.9 Kcal/mol) binding affinity with Mpro and formed hydrogen bonds at PHE140, ASN142, GLY143, SER144, CYS145 and GLU166.

This shares the same binding pocket with the standard (PHE140, GLY143, SER144, HIS 164A and GLU166) (Table 3, Figure 6).

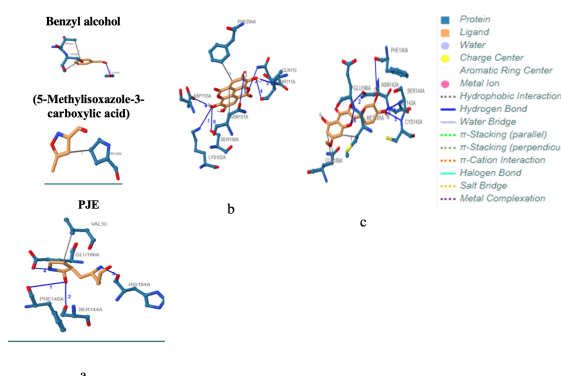


Figure 6. Protein-Ligand interactions of MPro of SARS-CoV-2 with standard and lead compounds a: N3, b: Ellagic acid c: Rhamnetin

From the results obtained from *Fpocket* (Tables 4 & 5, Figure 7), this binding cavity is Pocket 2 and it is the active site of Mpro. This is because Pocket 2 is the largest binding pocket as it has the highest druggability score, total SASA, and pocket volume (49). Pocket 2 is also the only binding pocket that contains Cysteine and Histidine residues which are part of the catalytic subunit of the active site (50). Specifically, Rhamnetin binds with CYS145 which is part of the catalytic subunit of the active site and would hinder the catalytic activity of the enzyme.

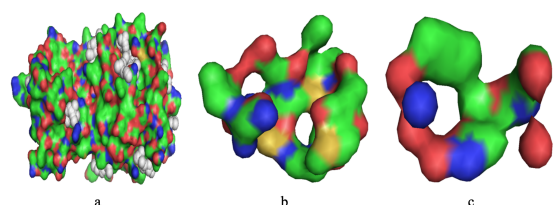


Figure 7. Crystal structure of MPro of SARS-CoV-2 showing the binding pockets (white balls) a: Whole protein, b: Active site (Pocket 2), c: Pocket 8 (binding site for Ellagic acid)

Ellagic acid exhibited (-8.3 Kcal/mol) binding affinity with 6LU7 and formed hydrogen bonds at LYS102, GLN110, THR111, ASN151, ASP153, and SER158 within Pocket 8 which is not the Mpro active site (Table 4 & 5, Figure 7; Table 1S is provided as the supporting information). In drug development, the other adjoining pockets to the binding site may also be recruited for ligand design (51). Some natural compounds which have been identified as potential inhibitors of Mpro also interact through Pocket 8 suggesting that they are allosteric inhibitors. The

compounds include Rein, Withanolide D, Withaferin A and Enoxacin (16).

Table 4. Parameters of binding pockets of the crystal structure of Mpro

Pocket parameters	Binding pockets												
	1	2	3	4	5	6	7	8	9	10	11	12	13
Pocket Score	0.12	0.11	0.09	0.06	0.06	0.03	0.02	0.01	-0.01	-0.02	-0.06	-0.09	-0.13
Druggability Score	0.01	0.19	0.00	0.00	0.01	0.01	0.02	0.00	0.00	0.00	0.00	0.00	0.00
Number of Alpha Spheres	20.00	104.00	21.00	20.00	15.00	25.00	29.00	21.00	16.00	15.00	16.00	23.00	16.00
Total SASA	89.90	270.31	63.99	48.82	74.50	64.60	109.66	80.28	57.49	46.49	94.04	114.48	99.60
Polar SASA	24.69	120.58	33.64	25.87	22.57	25.96	42.03	47.68	24.89	35.62	43.32	71.00	47.68
Apolar SASA	65.21	149.73	30.35	22.95	51.93	38.64	67.63	32.61	32.61	10.87	50.72	43.48	51.93
Pocket Volume	401.32	1134.13	276.00	213.29	308.49	246.51	427.76	234.59	223.85	169.60	226.25	376.09	279.28
Mean local hydrophobic density	7.00	31.11	2.00	7.00	8.00	16.00	14.63	9.00	5.00	2.00	0.00	7.00	1.00
Mean alpha sphere radius	4.02	4.03	3.97	3.97	4.07	4.04	4.08	3.81	4.18	4.04	3.85	3.86	4.01
Mean alp. sph. solvent access	0.76	0.50	0.57	0.60	0.60	0.63	0.49	0.51	0.66	0.63	0.51	0.43	0.55
Apolar alpha sphere proportion	0.40	0.37	0.14	0.40	0.60	0.68	0.55	0.48	0.38	0.20	0.06	0.35	0.13
Hydrophobicity score	31.56	19.60	20.56	40.13	32.17	5.50	22.50	25.22	26.50	-18.43	8.67	4.67	32.71
Amino Acid based Volume score	2.89	4.10	3.33	5.50	4.67	3.83	3.75	3.89	4.60	3.86	3.00	3.58	4.71
Polarity score	3.00	12.00	5.00	5.00	2.00	4.00	5.00	6.00	6.00	5.00	5.00	6.00	4.00
Charge score	-1.00	2.00	1.00	1.00	1.00	3.00	0.00	-1.00	0.00	-1.00	0.00	-1.00	2.00
Proportion of polar atoms	40.91	39.66	58.82	38.89	33.33	33.33	33.33	47.62	44.44	53.85	56.25	40.00	57.14
Alpha sphere density	4.58	6.29	3.10	2.26	3.63	2.35	3.90	3.01	2.10	1.56	3.11	3.26	2.65
Cent. of mass - Alpha Sphere max dist.	9.60	17.30	6.29	5.21	8.50	5.14	10.09	6.92	4.59	2.81	7.88	6.90	6.64
Flexibility	0.57	0.47	0.75	0.54	0.53	0.49	0.66	0.56	0.76	0.80	0.45	0.41	0.65

Table 5. Analysis of residues of binding pockets of the crystal structure of Mpro

Binding pockets		1	2	3	4	5	6	7	8	9	10	11	12	13		
THR	HIS	CYS	PHE	3	PHE	VAL	GLU	PHE	8	TRP	ASP	48	ASN	GLN	ASN	63
224	41	22			8	35	14			218		133	107			
VAL	MET	GLY	ARG	4	PRO	GLY	GLN	GLY	GLN	PHE	ASN	THR	PRO	HIS	64	
247	49	23			9	79	15	110		219	51	135	108			
GLY	TYR	THR	LYS	5	GLY	HIS	MET	THR	111	ASN	PRO	LYS	GLY	PHE	66	
251	54	24			11	80	17			221	52	137	109			
SER	PHE	THR	TRP		LYS	SER	81	TRP	ASN	PHE	ASN	53	THR	GLN	GLN	74
254	140	25	207		12		31	31	151	223		169	110			
ALA	LEU	ILE	LEU	282	ILE	LYS	88	ALA	ILE	GLU	ASP	56	VAL	ILE	LEU	75
255	141	43			152			70	152	270		171	200			
ALA	ASN	CYS	SER		TYR	LYS		GLY	ASP	153	LEU	LEU	ALA	VAL	ARG	76
260	142	44	284		154	90		71		271	57	193	202			
VAL	GLY	THR	GLU					VAL	SER	158	ASN	ARG	ALA	ASN	VAL	77
261	143	45	288					73		274	60	194	203			
LEU	SER	LYS	PHE					LEU	THR	292	GLY	GLY	GLU			
262	144	61	291					75		275		195	240			
ASP	CYS	ASN						THR	PHE	294	ASN	ASP	ASP			
263	145	65						93		277		197	245			
	HIS							ASN		279			HIS			
	163							95					246			
	HIS							PRO					ILE			
	164							96					249			
	MET							LYS					PRO			
	165							97					293			
	GLU							166								
	LEU							167								
	PRO							168								
	ASP							187								
	ARG							188								
	GLN							189								
	THR							190								
	GLN							192								

Mpro contains three domains namely Domains I (residues 8-101), and Domain II (residues 102-184) and Domain III (185-306) (51). While Rhamnetin and N3 bind at the active site in Domain II, Ellagic acid binds at another pocket (pocket 8 which might be an

allosteric site) in the same domain (Tables 4 & 5, Figure 7). Since cysteine proteases are allosteric enzymes, Pocket 8 or any other binding pocket apart from the active site could exhibit cooperativity (52).

The average donor to acceptor distance and bond angles for all the residues in the Mpro-Rhamnetin complex is shorter and smaller than in the Mpro-N3 complex. This data suggests that Mpro-Rhamnetin complex has stronger hydrogen bonding than the Mpro-N3 complex (Table 3).

Molecular Dynamic Simulation Analyses

The conformations induced by Ellagic acid and Rhamnetin closely resemble each other and show greater distortion from the Apo structure than the conformation induced by the standard (Figure 8).

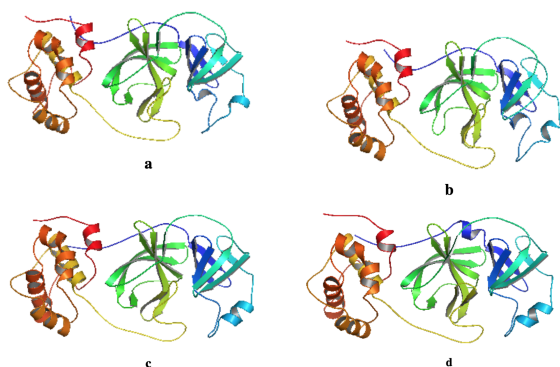


Figure 8. Structure of Apo and Holo proteins obtained after molecular dynamic simulation of a: Mpro, b: Mpro- N3 complex, c: Mpro-Ellagic acid complex & d: Mpro-Rhamnetin complex

Principal components Analysis: The statistical correlation between conformations obtained during the trajectory are determined with the Principal Component Analysis (PCA) (53). During the trajectory, the motions of all the Apo and Holo structures identifies the differences in their conformations. Data for these differences was obtained from the global (total and average) and the regional (total and average) motions of the principal components. For this study, the regional data was obtained from the 20 residues domiciled in the Mpro active site (Pocket 2).

Averagely, the Mpro-Rhamnetin (PC1, PC2 and PC3) shows the greatest motion of its global structure as compared with the other complexes. Specifically, as compared with the Apo structure, PC1 of the Mpro-Rhamnetin complex shows the greatest distortion. The Mpro-N3 complex shows greater distortion than the Mpro-Ellagic acid complex when compared to the

reference Apo structure (Table 1S). On the contrary, the regional (total and average) motions for the Mpro-N3 and Mpro-Ellagic acid complexes are greater than those of the Mpro- Rhamnetin complex. This suggests that N3 and Ellagic acid show slightly greater distortion of the Mpro active site than Rhamnetin (Table 1S).

The five ensembles (PC 1-5) for Mpro, Mpro-N3 complex, Mpro-Ellagic acid complex and Mpro-Rhamnetin complex have a total proportion of variance of 78.4%, 72.6%, 75.8%, and 78.4% respectively (Figure 9). The ensemble distribution of the Mpro-Rhamnetin complex most closely resembles that of the Apo structure and has the highest proportion of variance.

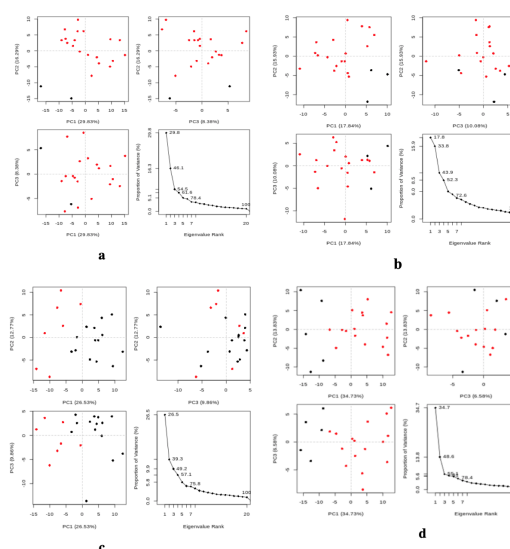


Figure 9. PCA cluster plot of Apo and Holo proteins a: Main protease, b: Main protease- N3 complex, c: Main protease-Ellagic acid complex & d: MPro- Rhamnetin

Root Mean Square Deviation of Atomic Positions (RMSD): The RMSD measures the differences in coordinates between a target structure when it is superimposed with a reference structure. A value of zero shows a perfect overlap (54).

The simulated Apo protein as compared with the crystal structure suggests there is a gradual increase in RMSD until it peaks (2.07Å) around 700ps when it then commences a gentle decline throughout the simulation period. The RMSD values of the simulated Mpro-N3 complex peaks (1.44Å) around 2,000ps and shows a gentle increase throughout the trajectory. While, the RMSD value of the simulated Mpro-Rhamnetin complex generally rises throughout the trajectory, it attains its peak (1.98Å) at about 1,100ps.

The simulated Mpro-Ellagic acid complex maintains a relative stability (at about 1.2 Å) in RMSD values throughout the trajectory but peaks (1.48Å) at 600ps (Table 6, Figure 10).

Table 6. RMSD values for Apo and Holo structures for 20 Frames (2 ns)

Time frame	Mpro	Mpro-N3	Mpro-Ellagic acid	Mpro-Rhamnetin
1	0.00	0.00	0.00	0.00
2	1.30	1.25	1.16	0.91
3	1.49	1.18	1.24	1.20
4	1.84	1.12	1.23	1.16
5	1.70	1.06	1.31	1.41
6	1.82	1.30	1.48	1.40
7	2.07	1.35	1.43	1.38
8	2.05	1.32	1.27	1.34
9	1.90	1.07	1.19	1.40
10	1.60	1.03	1.35	1.87
11	1.48	1.11	1.30	1.98
12	1.33	1.35	1.23	1.47
13	1.38	1.18	1.19	1.41
14	1.42	1.20	1.22	1.48
15	1.33	1.06	1.20	1.47
16	1.54	1.32	1.27	1.61
17	1.57	1.26	1.26	1.86
18	1.70	1.23	1.23	1.51
19	1.49	1.29	1.25	1.58
20	1.30	1.44	1.20	1.81
21	1.34	1.36	1.24	1.85

Total	31.64	24.49	25.24	30.09
Range	0-2.07	0-1.44	0-1.48	0-1.98
Average	1.51	1.17	1.20	1.43

Each time frame is equivalent to 100 ps

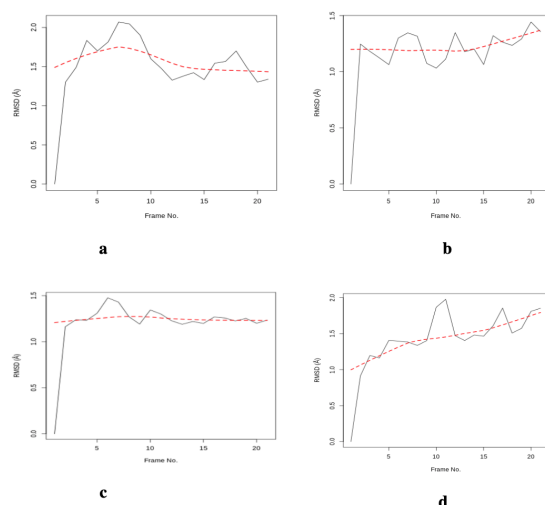


Figure 10. RMSD of Apo and Holo proteins a: Main protease, b: Mpro- N3 complex, c: Mpro-Ellagic acid complex & d: Mpro-

Rhamnetin

During the trajectory, the total, average and range of RMSD values of the Mpro-Rhamnetin complex is the highest. The Mpro-Ellagic acid complex also shows greater value than the Mpro-N3 complex (Table 5). Furthermore, the distribution of the peaks in the RMSD histogram (Figure 11) suggests that the Mpro-N3 complex has its peaks between 1.0-1.5 Å; the Mpro-Ellagic acid complex lies between 1.2-1.5 Å; and the Mpro-Rhamnetin complex has its peaks between 1.0- 2.0 Å.

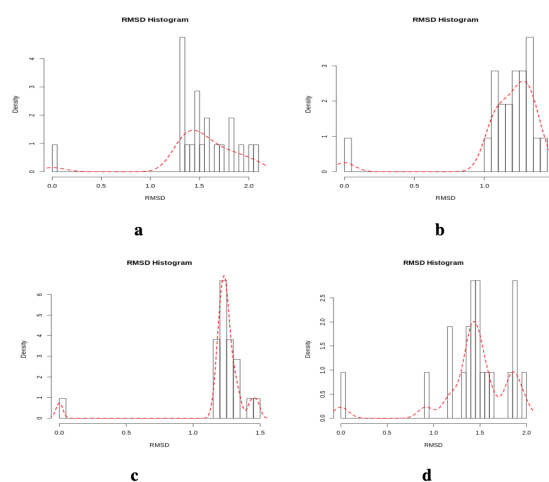


Figure 11. RMSD histogram of Apo and Holo proteins a: Mpro, b: Mpro- N3 complex, c: Mpro- Ellagic acid complex & d: Mpro-Rhamnetin complex

Put together, predictably, Rhamnetin induces the greatest distortion of the global structure of Mpro. This is because during the trajectory, the RMSD of Mpro-Rhamnetin complex shows steep ascendancy (as compared with gentle ascendancy of the Mpro-N3 complex). Mpro-Rhamnetin complex also shows the highest instability as revealed in the total, average and range of RMSD values. The highest instability is also seen in Mpro-Rhamnetin complex as revealed in the range of RMSD values seen in the histogram (Figure 11).

Root Mean Square Fluctuations (RMSF): Under different physiological, pathological and pharmacological conditions proteins undergo fluctuations over a range of time scales. The RMSF measures the fluctuations of the carbon alpha atom of residues around their equilibrium conformations (55).

The Mpro-Rhamnetin complex showed the greatest fluctuations in its global structure. The Mpro-Ellagic acid complex also showed greater fluctuations in its

global structure than the Mpro-N3 complex. On the contrary, the regional fluctuations of the Mpro active site reveals that the greatest fluctuation was induced by N3. Ellagic acid also induced a slightly more fluctuation than Rhamnetin at the Mpro active site (Table 2S, Figure 12).

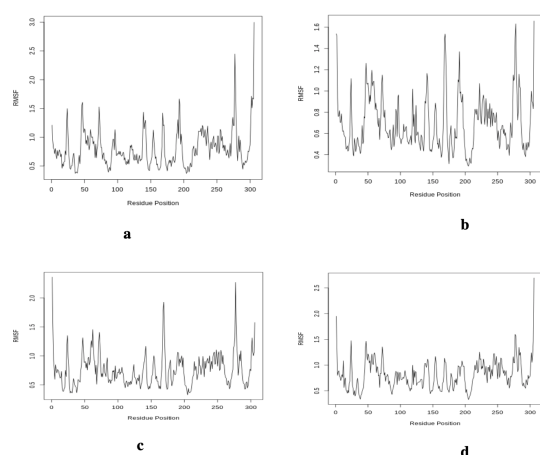


Figure 12. Per-residue RMSF of Apo and Holo proteins a: Main protease, b: Main protease- N3 complex, c: Main protease-Ellagic acid, d: Main protease-Rhamnetin

EXPERIMENTAL

Data source: In this study, a library of 1,048 Lipinski and Veber rule-compliant bioactive compounds was used. The compounds were obtained from edible African plants which are fruits, vegetables and spices. The 3D SDF structures of the natural compounds were downloaded from *Pubchem* (24).

Preparation and structural analysis of target protein structure: The 3D conformer of the crystal structure of COVID-19 Main Protease in complex with an inhibitor N3 (PDB ID: 6LU7) was downloaded from the RCSB Protein Data Bank (23, 25). The co-crystallized ligand and water molecules attached to the protein was removed by a visualization tool, *Pymol* (26). To reduce the steric clashes of the protein structure, *Chiron*, an online server was used for the energy minimization (27). The Ramachandran plot of the target protein was obtained using *VADAR* (Volume, Area, Dihedral Angle Reporter) online server (28).

Molecular docking **Molecular docking:** All the ligands were loaded on the Python prescription software (*PyRx* 0.8 version) and converted from SDF to pdbqt format in the preparation for molecular docking (29). The Universal Force Field (UFF) was

used as the energy minimization parameter and conjugate gradient descent as the optimization algorithm. The target protein was docked against ligands using the following grid parameters, Centre: X= -26.284, Y= 12.596, Z= 58.9679 and Dimensions (Angstrom): X= 51.3732, Y=66.9737, Z=59,6071. **Screening:** Ligands with the maximum binding affinity were selected using the docking results (-7.4 kcal/mol) of the reference compound, N3 as cut-off. Ligands were further screened for molar refractivity using the *SWISSADME* server (30). Prediction for pharmacokinetic properties and bioactivity were done using the *pkCSM* and *Molinspiration* respectively (31, 32). An online SMILES generator, the *CACTUS* web server was used to generate the SMILES for N3 (33).

Binding site analyses: Protein-Ligand Interaction Profiler webserver was used to reveal the binding site of Mpro and all ligand interactions. The analyses include the exhaustiveness, name and number of residues, bond distance and bond angle (34). The *Fpocket* webserver was also used to analyze all the binding pockets of the target protein (35).

Molecular Dynamics Simulations: The Galaxy (versions 2019.1 and 2019.1.4) supercomputing server which uses the Groningen Machine for Chemical Simulations (GROMACS) software was used for the molecular dynamics simulation of the Apo and Holo protein structures (36, 37). For Ligand parameterization, *LigParGen* was used to generate GROMACS-compatible topology files for the small molecules. OPLS-AA/1.14*CM1A was the force field parameter used (38). For the set-up of the initial simulation, the parameters used include: OPLS/AA force field, SPC/E water model, rectangular box type with all equal sides measuring 1.5nm each and Hydrogen was ignored. The SPC water model was used for solvation and the addition of ions. For energy minimization, the steepest descent algorithm was used for 50,000 steps. 1.0 was used for all the Distance cut-offs (include for short range van der Waals, Coulomb, and the short-range neighbor). Fast smooth Particle-Mesh Ewald electrostatics and EM tolerance of 1000 were used as other energy minimization parameters.

NVT and NPT equilibration was performed with the following parameters: 0.002 ps step length, 5,000 steps between saving data points, 300k temperature, leap-frog integrator, and constrained Bonds with H-atoms. Finally, a 2ns molecular dynamics simulation of the Apo and Holo structures was performed using 1,000,000 steps. Analyses of trajectories were done using the BIO 3D tool on the Galaxy super-computing

platform (39). These include the Principal Component Analysis (PCA), Root Mean Square Fluctuation (RMSF) of protein backbone, and Root Mean Square Deviation of atomic positions (RMSD) (37).

CONCLUSION

The Mpro is an essential enzyme for the proteolytic maturation of the coronavirus. Hence it has become therapeutic target in combating COVID-19. After docking 1,048 natural compounds against Mpro and screening for good pharmacokinetic properties and bioactivity, two lead compounds namely Ellagic acid and Rhamnetin were identified. Overall, the lead compounds proved to be better drug candidates than the standard in terms of bioavailability and pharmacokinetic properties.

Rhamnetin interacted directly on the active site suggesting a competitive inhibition of Mpro while Ellagic acid interacted at a suspected allosteric site (in the same domain) just like some other natural compounds, Rein, Withanolide D, Withaferin A and Enoxacin (16). Though the standard is predicted to have a better protease inhibition activity, the lead compounds excel in terms of general enzyme inhibition. The molecular dynamics calculations confirm that Rhamnetin induces the greatest instability of the Mpro global conformation suggesting the greatest inhibitory effect. However, at the active site, Ellagic acid induces slightly greater motions than Rhamnetin as revealed by the PCA and RMSF values. This suggests that though Ellagic acid does not bind at the Mpro active site, it probably has an allosteric effect on it.

Ellagic acid is a polyphenol found in several fruits such as walnut, grapes and strawberries (56). It inhibits the replication of Human rhinoviruses HRV-2, and HRV-3) which are also single-stranded positive-sense RNA viruses that are also a major cause of common cold (57). As part of the extract of *Rhodiolarosea*, Ellagic acid displayed specific and potent inhibition against the cell entry of both Ebola and Marburg viruses. (58). The antiviral activity of Ellagic acid has also been demonstrated against high-risk Human Papilloma Virus (59).

The antiviral activity of Rhamnetin which is an O-methylated flavonol found in cloves has also been established. Rhamnetin is an inhibitor of Neuroinvasive West Nile virus replication and another derivative, isorhamnetin has potent effect against the influenza virus (60, 61). A combination of eugenol and

rhamnetin both isolated from cloves exhibited inhibitory activity against Influenza H1N1, Hepatitis-B/C, Zika, Dengue, CMV, HIV-1, SFV, Sindbis, respiratory syncytial, and Ebola viruses (62).

It is recommended that the inhibitory effect of Rhamnetin on the active site should be further investigated. The possible allosteric effect of Pocket 8, where Ellagic binds on the structure and function of the Mpro active site should also be determined. While Rhamnetin has to go through the rigorous process of drug development, Ellagic acid is readily available as commercial food supplements making clinical trials easier.

Acknowledgements

The authors wish to thank the management of the Department of Medical Biotechnology, National Biotechnology Development Agency, Abuja, Nigeria for providing an enabling environment for this research.

Bibliography

1. Mahtani, S., Berger, M., O'Grady, S., & Iati, M. (2020). "Hundreds of evacuees to be held on bases in California; Hong Kong and Taiwan restrict travel from mainland China". *The Washington Post*. Archived from the original on 7 February 2020.
2. World Health Organization. (2020) "Naming the coronavirus disease (COVID-19) and the virus that causes it". Archived from the original on 28 February 2020.
3. Velavan, T.P., & Meyer, C.G. (2020). "The COVID-19 epidemic". *Tropical Medicine & International Health*. n/a (n/a): 278–80.
4. Centers for Disease Control and Prevention United States. (2020) "Coronavirus Disease 2019 (COVID-19) Symptoms" Archived from the original on 30 January 2020.
5. Cascella, M., Michael, R., Arturo C., Scott C. D., R, D.N. (2020) Features, Evaluation and Treatment Coronavirus (COVID-19). StatPearls Publishing Treasure Island (FL)
6. Poon, L. M., & Peiris, M. 2020. Emergence of a novel human corona virus threatening human health. *Journal of Nature Medicine*, 26(3): 317–319.
7. Pillaiyar, T., Meenakshisundaram, S., & Manickam, M. (2020). Recent discovery development of inhibitors targeting coronaviruses. *Journal of Drug Discovery today*. S1359-6446(20)30041-6.
8. Lau SKP, Wong EYM, Tsang CC, Ahmed SS, Au-Yeung RKH, Yuen KY, Wernery U, Woo PCY (2018). Discovery and Sequence Analysis of Four Deltacoronaviruses from Birds in the Middle East Reveal Interspecies Jumping with Recombination as a Potential Mechanism for Avian-to-Avian and Avian-to-Mammalian Transmission. *J Virol*. 92(15).
9. Poon, L. L., Guan, Y. J., Nicholls, M., Yuen, K.Y., & Peiris, J. S., 2004. The aetiology, origins, and diagnosis of severe acute respiratory syndrome. *Lancet Infect. Dis*. 4:663–671.

10. Zhong, N. S., Zheng, B.J., Li, Y. M., Poon, Z. H., Xie, K. H., Chan, P. H., Guan, Y. (2003). Epidemiology and cause of severe acute respiratory syndrome (SARS) in Guangdong, People's Republic of China, in February, 2003. *Lancet* 362:1353–1358.
11. Poon, L. L., Wong, O. K., Chan, K. H., Luk, W., Yuen, K.Y., Peiris, J. S., & Guan, Y. (2003). Rapid diagnosis of a coronavirus associated with severe acute respiratory syndrome (SARS). *Clin. Chem.* 49:953–955
12. Letko M., Marzi A., & Munster V. (2020). "Functional assessment of cell entry and receptor usage for SARS-CoV-2 and other lineage B betacoronaviruses". *Nature Microbiology*: 1–8.
13. Tai, W., Lei, H., Xiujuan, Z., Jing, P., Denis, V., Shibo, J., Yusen, Z., & Lanying, D. (2020). Characterization of the receptor-binding domain (RBD) of 2019 novel coronavirus: implication for development of RBD protein as a viral attachment inhibitor and vaccine. *Cellular & Molecular Immunology*.
14. Graham, R.L., & Baric R. S. (2010). "Recombination, Reservoirs, and the Modular Spike: Mechanisms of Coronavirus Cross-Species Transmission," *J. Virol.*
15. Hurst, K.R., Kuo L., Koetzner, C. A., Ye, R., Hsue, B., & Masters, P.S. (2005). "A Major Determinant for Membrane Protein Interaction Localizes to the Carboxy-Terminal Domain of the Mouse Coronavirus Nucleocapsid Protein," *J. Virol.*
16. Chandel, V., Raj, S., Rathi, B., Kumar, D. (2020). In Silico Identification of Potent COVID-19 Main Protease Inhibitors from FDA Approved Antiviral Compounds and Active Phytochemicals through Molecular Docking: A Drug Repurposing Approach. *Preprints* 2020030349.
17. Patick, A. K., & Potts, K.E. (1998). Protease Inhibitors as Antiviral Agents. *Clin Microbiol Rev.* 11(4): 614–627.
18. Vicik, R., Busemann, M., Baumann, K., Schirmeister, T. (2006). Inhibitors of cysteine proteases. *Curr Top Med Chem.* 6(4):331-53.
19. Liu, X., Alexander, G., Pavlovsky, & Ronald, E. V. (2008). The Structural Basis for Allosteric Inhibition of a Threonine-sensitive Aspartokinase. *J Biol Chem.* 283(23): 16216–16225.
20. Dhillon, A., Sharma, K., Rajulapati, V., Goyal, A. (2017) Current Developments in Biotechnology and Bioengineering: Production, Isolation and Purification of Industrial Products. Indian Institute of Technology Guwahati, Guwahati, Assam, India.
21. David, G. (2020). Coronary virus proteases. RCSB PDB-101 Molecular explorations through biology and medicine. <https://pdb101.rcsb.org/motm/242> doi:10.2210/rcsb_pdb/mom_2020_2
22. Cui, J., Li, F., Shi, Z.L. (2019) Origin and evolution of pathogenic coronaviruses. *Nat. Rev. Microbiol.* 17, 181-192.
23. Liu, X., Zhang, B., Jin, Z., Yang, H., Rao, Z. (2020). RCSB Protein Data Bank, 162043 Biological Macromolecular Structures Enabling Breakthroughs in Research and Education.
24. Kim, S., Chen, J., Cheng, T., Gindulyte, A., He, J., He, S., Li, Q., Shoemaker, B. A., Thiessen, P. A., Yu, B., Zaslavsky, L., Zhang, J., & Bolton, E. E. (2019). PubChem 2019 update: improved access to chemical data. *Nucleic acids research*, 47(D1), D1102–D1109.
25. Berman, H.M., Westbrook, J., Feng, Z., Gilliland, G., Bhat, T.N., Weissig, H., Shindyalov, I.N., & Bourne, P.E. (2000) The Protein Data Bank *Nucleic Acids Research*, 28: 235-242.
26. DeLano, W.L. (2002) The PyMOL Molecular Graphics System. Delano Scientific, San Carlos.
27. Ramachandran, S., Kota, P., Ding, F. & Dokholyan, N. V. (2011). PROTEINS: Structure, Function and *Bioinformatics*, 79: 261-270 (2011)
28. Willard, L., Anuj, R., Haiyan, Z., Hassan, M., Robert, F. B., Brian, D., Sykes., & David S. W. (2003). VADAR: a web server for quantitative evaluation of protein structure quality. *Nucleic Acids Res.* 31(13): 3316–3319.
29. Dallakyan, S. & Olson, A J. (2015). Small-molecule library screening by docking with PyRx. *Methods Mol Biol.*; 1263:243-50.
30. Daina, A., Olivier, M., & Vincent, Z. (2017). SwissADME: a free web tool to evaluate pharmacokinetics, drug-likeness and medicinal chemistry friendliness of small molecules. *Sci Rep.* 7: 42717
31. Pires, D.E.V., Tom, L., Blundell, D. B., Ascher. (2015). pkCSM: predicting small-molecule pharmacokinetic properties using graph-based signatures. *Journal of Medicinal Chemistry*, 58 (9): 4066–4072.
32. Molinspiration (2015) Calculation of Molecular Properties and Bioactivity Score.
33. <http://www.molinspiration.com/cgi-bin/properties>.
34. National Cancer Institute. (2020). Online SMILES Translator and Structure File Generator, CADD Group, NCI, National Institute of Health.
35. Salentin, S., Schreiber, S., Haupt, V.J., Adasme, M.F, Schroeder, M. (2015) PLIP: fully automated protein-ligand interaction profiler. *Nucleic Acids Res.* 43(W1): W443-7.
36. Guilloux, L.V., Peter, S., & Pierre T. (2009) "Fpocket: An open source platform for ligand pocket detection", *BMC Bioinformatics*, 10:168
37. Abraham, M.J., R, S., SzilárdPáll, J. C., SmithBerk, H.E. (2015) GROMACS: High performance molecular simulations through multi-level parallelism from laptops to supercomputers. *Software X* Volumes 1–2, Pages 19-25.
38. Afghan, E., Dannon, B., Marius, V.B., Daniel, B., Dave, B., Martin, Č., John, C., Dave, C..... Jeremy, G. (2016). The Galaxy platform for accessible, reproducible and collaborative biomedical analyses: update, *Nucleic Acids Research* 44(W1): W3-W10
39. Dodda, L.S., Cabeza, V. I., Tirado-Rives, J., Jorgensen, W.L. (2017). LigParGen web server: an automatic OPLS-AA parameter generator for organic ligands. *Nucleic Acids Res.* 3;45(W1): W331-W336.
40. Grant, B. J., Rodrigues, A. P. C., ElSawy, K. M., McCammon, J. A., & Caves, L. S. D. (2006). Bio3d: An R package for the comparative analysis of protein structures. In *Bioinformatics*, 22 (21), pp. 2695-2696
41. Lipinski C. A., Lombardo F., Dominy B. W., & Feeney, P. J. (2001). Experimental and computational approaches to estimate solubility and permeability in drug discovery and development settings. *Adv. Drug. Deliv. Rev.* 46, 3–26
42. Veber, D.F., Johnson, S.R, Cheng, H.Y., Smith, B.R., Ward, K.W., Kopple, K.D. (2002) Molecular properties that influence the oral bioavailability of drug candidates. *J Med Chem.* 6;45(12):2615-23.
43. Ghose, A.K, Viswanadhan, V.N., Wendoloski, J.J (1999). A knowledge-based approach in designing combinatorial or medicinal chemistry libraries for drug discovery. A qualitative and quantitative characterization of known drug databases. *J Comb Chem.* 1(1):55-68.
44. Khan Tahmeena, Shalini Dixit, Rumana Ahmad, Saman Raza, Iqbal Azad, Seema Joshi, and Abdul Rahman Khan. (2017): Molecular docking, PASS analysis, bioactivity

- score prediction, synthesis, characterization and biological activity evaluation of a functionalized 2-butanone thiosemicarbazone ligand and its complexes. *J Chem Biol.* 10(3): 91–104.
45. Guan, L., Hongbin, Y., Yingchun, C., Lixia, S., Peiwen, D.W. L., Guixia, L., & Yun, T. (2019). ADMET-score – a comprehensive scoring function for evaluation of chemical drug-likeness. *Medchemcomm.* 10(1): 148–157.
 46. Pires, E. V. D., Tom L. B., & David, B. A. (2015) pkCSM: Predicting Small-Molecule Pharmacokinetic and Toxicity Properties Using Graph-Based Signatures. *J Med Chem.* 58(9): 4066–4072.
 47. Kim, B. R. (2002). Drugs as P-glycoprotein substrates, inhibitors, and inducers *Drug Metabolism Reviews* . Volume 34, [Issue 1-2](#)
 48. Sanguinetti, M.C., Tristani-Firouzi, M. (2006). "hERG potassium channels and cardiac arrhythmia". *Nature.* 440 (7083): 463–9.
 49. Du, X., Yi, L., Yuan-Ling, X., Shi-Meng, A., Jing, L., Peng, S., Xing-Lai, J. & Shu-Qun, L. (2016). Insights into Protein–Ligand Interactions: Mechanisms, Models, and Methods. *Int J Mol Sci.* 17(2): 144.
 50. Liang, J., Edelsbrunner, H., & Woodward, C. (1998). Anatomy of protein pockets and cavities: measurement of binding site geometry and implications for ligand design. *Protein Sci.* 7(9): 1884–1897.
 51. Anand, K., Gottfried, J., Palm, J. R., Mesters, S.G., Siddell, J. Z., & Rolf, H. (2002) Structure of coronavirus main proteinase reveals combination of a chymotrypsin fold with an extra α -helical domain. *EMBO J.* 21(13): 3213–3224.
 52. Tian, S. P. S., Meng, Z., Yang, L. (2020): Insight Derived from Molecular Docking and Molecular Dynamics Simulations into the Binding Interactions Between HIV-1 Protease Inhibitors and SARS-CoV-2 3CLpro. *ChemRxiv. Preprint.*
 53. Sanchez, M. I., De Vries, L.E., Lehmann, C., Lee, J.T, Ang, K.K., Wilson, C., et al. (2019) Identification of Plasmodium dipeptidyl aminopeptidase allosteric inhibitors by high throughput screening. *PLoS ONE* 14(12): e0226270
 54. David CC and Jacobs DJ (2014): Principal component analysis: a method for determining the essential dynamics of proteins. *Methods Mol Biol.* 1084:193-226.
 55. Kufareva, I., & Abagyan, R. (2012). Methods of protein structure comparison. *Methods Mol Biol.* 857: 231–257.
 56. Fuglebakk, E., Julián, E., & Nathalie, R. (2012). Measuring and comparing structural fluctuation patterns in large protein datasets. *Bioinformatics.* 28 (19): 2431–2440
 57. Vattem, D. A., & Shetty, K. (2005). "Biological Function of Ellagic Acid: A Review". *Journal of Food Biochemistry.* 29 (3): 234–266.
 58. Sang, W. P., Min, J. K., Ji Young, Y., Hwa-Jung, C., & Young-Joon, A. (2014) Antiviral activity and possible mode of action of ellagic acid identified in *Lagerstroemia speciosa* leaves toward human rhinoviruses. *BMC Complement Altern Med.* 14: 171.
 59. Cui, Q., Ruikun, D., Manu, A., Adam, S., Lin, H., Jingzhen, T., Robert, A. D., Han, C., & Lijun, R. (2018). Identification of Ellagic Acid from Plant *Rhodiarosea* L. as an Anti-Ebola Virus Entry Inhibitor. *Viruses* 10(4):152
 60. DonnMaria,L., Lentini, M., Alibrandi, A., Salimbeni, V., Giuffre, G., Mazzeo, F., Triolo, O.,& D'Anna, R. (2017) Antiviral activity of Ellagic acid and Annona Muricata in cervical HPV related pre-neoplastic lesions: A randomized trial. *Journal of Functional Foods* [Volume 35](#), Pages 549-554
 61. Boominathan, L. (2017) Natural product-derived antiviral therapy against Neuroinvasive West Nile virus: Rhamnetin, an O-methylated flavonol found in Cloves, increases the expression of RIPK3, promotes chemokines production, inhibits neuroinflammation, and restricts neuroinvasive West Nile virus production and pathogenesis in neurons via up regulation of its target gene,Genome-2-Bio-Medicine Discovery center (GBMD), <http://genomediscovery.org>
 62. Daye m, A. A., Hye, Y. C., Young, B. K., Ssang-Goo, C. (2015) Antiviral Effect of Methylated Flavonol Isorhamnetin against Influenza *PLoS One.* 10(3): e0121610.
 63. Boominathan, L. (2018). Anti-infective Therapy: A therapeutic mix encompassing eugenol and rhamnetin, isolated from cloves, inhibits Hepatitis-B/C, Dengue, Zika, Ebola, HIV-1, Mtb, Malaria, CMV, Influenza H1N1, respiratory syncytial, Sindbis, and SFV viruses by increasing the Levels of the Antiviral Proteins IFITM3, & Interferon-stimulated gene 15, 20/March/2018, 10.54 pm

Affiliations and Corresponding Informations

Corresponding: Adekunle Babajide Rowaiye

Email: adekunlerowaiye@gmail.com

Phone:



Adekunle Babajide Rowaiye:

Department of Medical Biotechnology, National Biotechnology Development Agency, Lugbe, Abuja, Nigeria.



Olukemi Adejoke Onuh:

Department of Medical Biotechnology, National Biotechnology Development Agency, Lugbe, Abuja, Nigeria.



Rita Maneju Sunday:

Department of Medical Biotechnology, National Biotechnology Development Agency, Lugbe, Abuja, Nigeria.



Zainab Dauda Abdulmalik:

Department of Medical Biotechnology, National Biotechnology Development Agency, Lugbe, Abuja, Nigeria.



Doofan Bur:

Department of Medical Biotechnology, National Biotechnology Development Agency, Lugbe, Abuja, Nigeria.



Nkoli Winifred Emeter:

Department of Medical Biotechnology, National Biotechnology Development Agency, Lugbe, Abuja, Nigeria.



Oluwaseun Adeola Obideyi:

Department of Medical Biotechnology, National Biotechnology Development Agency, Lugbe, Abuja, Nigeria.



Charles Diwani Pellettri:

Department of Medical Biotechnology, National Biotechnology Development Agency, Lugbe, Abuja, Nigeria.



Inikpi Rabi Ujah-Samuel:

Department of Medical Biotechnology, National Biotechnology Development Agency, Lugbe, Abuja, Nigeria.



Chiamaka Rosemary Iwuozor:

Department of Medical Biotechnology, National Biotechnology Development Agency, Lugbe, Abuja, Nigeria.



Priscilla Yahemba Aondona:

Department of Medical Biotechnology, National Biotechnology Development Agency, Lugbe, Abuja, Nigeria.



Victoria Onyayi Etalong:

Department of Medical Biotechnology, National Biotechnology Development Agency, Lugbe, Abuja, Nigeria.



Nuratu Yussuff:

Department of Medical Biotechnology, National Biotechnology Development Agency, Lugbe, Abuja, Nigeria.



Jude Nnamdi Akpa:

Department of Medical Biotechnology, National Biotechnology Development Agency, Lugbe, Abuja, Nigeria.